ature. Under low-voltage (200–1000 V) electron-beam excitation, efficiency increased with an increase in crystallite size and found to be independent of particle size. The higher efficiency measured for powders with larger crystallites was attributed to a reduction in the number of nonradiative sites on the surface and in grain boundaries. A model was developed to predict the low-voltage CL efficiency of oxide phosphors as a function of crystallite size, particle size, and excitation voltage. An equation for the efficiency was derived which includes the backscattering factor, γ, the fraction of radiative recombination sites, S, and the effect of SBEs. An expression for S as a function of crystallite size and the number of grain boundaries was derived from simple geometric considerations. Calculated values of S using this expression were found to increase with an increase in crystallite size but were independent of particle size. The number of absorbed electrons was adjusted to account for loss of efficiency due to SBEs. The model predicted efficiencies that were in very good agreement with experimental results. The predicted efficiencies at higher voltages (>3 kV) using this model also correlate very well with measured results. This is the first model of CL efficiency that includes the effects of crystallite size and SBEs.

Acknowledgments

The financial support of this work by the California MICRO Program and the Phosphor Technology Center of Excellence (PTCOE) at the Georgia Institute of Technology is gratefully acknowledged. Thanks are given to Robert Walko and Robert Mays of Sandia National Laboratories in Albuquerque for use of their phosphor characterization facility.

Manuscript submitted October 27, 1997; revised manuscript received March 18, 1998.

The University of California at San Diego assisted in meeting the publication costs of this article.

REFERENCES

1. K. A. Franz, W. G. Kehr, A. Siggel, and J. Wieczoreck, in *Ullmann's Encyclopedia of Industrial Chemistry*, Vol. A15, B. Elvers, S. Hawkins, and G. Schulz, Editors, A15, VCH Publishers, Weinheim, Germany (1985).
2. B. G. Yacobi and D. B. Holt, *Cathodoluminescence Microscopy of Inorganic Solids*, Plenum Press, New York (1990).
3. L. Ozawa, *Cathodoluminescence*, VCH Publishers, New York (1990).
4. G. F. J. Carlick, *Brit. J. Appl. Phys.*, **13**, 541 (1962).
5. J. D. Kingsley and G. W. Ludwig, *J. Electrochem. Soc.*, **117**, 353 (1970).
6. G. W. Ludwig and J. D. Kingsley, *J. Electrochem. Soc.*, **117**, 348 (1970).
7. G. Gergely, *J. Phys. Chem. Solids*, **17**, 112 (1960).
8. D. J. Robbins, *J. Electrochem. Soc.*, **127**, 2694 (1980).
9. M. L. F. Phillips, *Proc. SPIE*, **2408**, 201 (1994) SPIE-Int. Soc. Dpt. Eng.
10. J. McKittrick, B. Hoghooghi, W. Dubbelday, K. Kavanagh, K. Kinsman, L. Shea, and E. Sluzky, *Mater. Res. Soc. Proc.*, **348**, 519 (1994).
11. L. Ozawa and H. N. Hersh, *Phys. Rev. Lett.*, **36**, 683 (1976).
12. F. Morehead, *Phys. Rev. B.*, **17**, 3432 (1978).
13. K. Ohno and T. Abe, *J. Electrochem. Soc.*, **141**, 1252 (1994).
14. J. S. Yoo and J. D. Lee, *Asia Display*, 647 (1995).
15. T. Welker and H. T. Hintzen, Abstract 652, p. 973, *Electrochemical Society Extended Abstracts*, Vol. 91-2, Phoenix, AZ, October 13-17, 1991.
16. L. E. Shea, J. McKittrick, O. A. Lopez, and E. Sluzky, *J. Am. Ceram. Soc.*, **79**, 3257 (1996).
17. D. Balzar, *J. Appl. Crystallogr.*, **25**, 559 (1992).
18. G. Wyszecki and W. S. Stiles, *Color Science: Concepts and Methods, Quantitative Data and Formulae*, 2nd ed., p. 256, John Wiley and Sons, Inc., New York (1982).

Passivation of Cu by Sputter-Deposited Ta and Reactively Sputter-Deposited Ta–Nitride Layers

Jui-Chang Chuang and Mao-Chieh Chen*

Department of Electronics Engineering and Institute of Electronics, National Chiao-Tung University, Hsinchu 300, Taiwan

ABSTRACT

Sputter-deposited tantalum (Ta) and reactively sputter-deposited Ta–nitride films were studied with respect to the passivation capability against copper (Cu) oxidation in thermal O_2 ambient. A 200 Å Ta or Ta–nitride film was sputter-deposited on a 2000 Å Cu film using a Ta target in an Ar/N_2 gas mixture. With Ta passivation, Cu was not oxidized at temperatures up to 400°C, which can be further improved by using passivation of an amorphous Ta–nitride film deposited in an appropriate condition. The absence of long-range defects in the Ta–nitride film was presumably responsible for this improvement. However, sputtering-induced surface damage by excess N_2 in the sputter gas mixture may reduce the passivation capability of Ta–nitride films. When the passivated Cu was oxidized, the Cu oxides always resided in the top surface region. That is, in the oxidation process, Cu diffused through the defects of the passivation layers to the outer surface.

Introduction

Copper (Cu) has been extensively studied as a potential substitute for aluminum (Al) and Al-alloys in multilevel metallization of semiconductor devices.[1-3] Compared with Al and Al-alloys, Cu has some beneficial factors, such as lower bulk resistivity (1.7 vs. 2.7 and >4.0 $\mu\Omega$ cm),[1,4] higher electromigration resistance,[5] higher melting point,[4,6] and lower reactivity with commonly used diffusion barrier materials.[6,7] However, Cu is worse than Al and Al-alloy in some aspects, such as difficulty in dry etching,[8] poor adhesion to the dielectric layer,[1,2] easy diffusion in silicon and SiO_2,[9-13] deep-level trap in silicon, and Cu silicide formation at low temperatures. Thus, the use of barrier layers to reduce diffusion of Cu and to improve adhesion to dielectrics, especially SiO_2,[8,14-20] is of importance. The barrier/adhesion layers for Cu metallization have been extensively investigated and are mostly listed in Ref. 14.

It is well known that Cu oxidizes easily in air and in humid ambient[21-24] even at room temperature. This quality has deferred the application of Cu in integrated circuits. A proper technique of passivation against Cu oxidation must be developed for its widespread application.[25] Several passivation schemes to resist Cu oxidation in an oxidizing ambient have been studied,[1,2] ranging from self-aligned passivation by (Al, Mg),[26,27] (Ti, Cr),[28] and Nb,[29] or sidewall passivation[30,31] by Mo and TiN, formation of surface silicide,[32] and B-implantation into Cu.[33]

* Electrochemical Society Active Member.

Table I. Sputtering gas and nitrogen content for Ta and Ta–nitride films.

Sample identification	A (Ta)	B (Ta–nitride)	C (Ta–nitride)	D (Ta–nitride)
Ar/N_2 flow rates (sccm)	(12/0)	(12/3)	(12/5)	(12/12)
Nitrogen atomic concentration in Ta or Ta-nitride films (atom %)	—	23.5	30.5	30.5

In this study, thin films of tantalum (Ta) and Ta–nitrides are used as passivation layers against Cu oxidation, because Ta and Ta–nitrides are conductive[4] and chemically inert with Cu[4,6,7] and have low solid solubility in Cu.[6,17] In addition, Ta and Ta–nitride are capable of withstanding Cu diffusion[34–37] and do not form intermetallic compound at high temperatures. In the experiments conducted, sputtered Ta and reactively sputtered Ta–nitride films were deposited on the Cu surface to produce Ta or Ta–nitride covered $Ta/Cu/SiO_2/Si$ or Ta–nitride/$Cu/SiO_2/Si$ structure, and then the passivation capability of Ta and Ta–nitride films against Cu oxidation were investigated.

Experimental

For sample preparation, the starting materials were p-type, boron-doped, 3 in. diam Si wafers with nominal resistivity of 17–55 Ω cm. After initial RCA cleaning,[38] the Si wafers were thermally oxidized at 1050°C in steam atmosphere to grow a 5000 Å SiO_2. A Cu film 2000 Å thick was sputter–deposited on the oxide layer, which was followed by a 200 Å Ta or Ta–nitride film deposition on the Cu film. The Ta film was sputter–deposited using a pure Ta target (99.999% purity) in Ar ambient, while the Ta–nitride films were deposited by reactive sputtering using the same Ta target in a gas mixture of Ar and N_2 with various flow rates. All the gases used were of electronic grade.The base pressure of the deposition chamber was 5×10^{-7} Torr, and all films were sputtered at a pressure of 7.8 mTorr. The dc sputtering power was 150 W for all deposition of Ta and Ta–nitride films. Table I summarizes the sputtering gas and sample identification for the sputtered Ta and reactively sputtered Ta–nitride films. Percentage atomic concentrations of nitrogen determined from Auger electron spectroscopy (AES) analysis are also listed. All wafers were diced into 1.5 × 1.5 cm pieces for further treatment. To investigate the passivation capability of Ta and Ta–nitride films against Cu oxidation, the diced samples were thermally annealed in flowing O_2 furnace for 50 min at temperatures ranging from 100 to 600°C. Electrical measurement and material analysis were used to characterize the passivation capability. Sheet resistance (*Rs*) was measured using a four-point probe. Scanning electron microscopy (SEM) was used to investigate surface morphology. X-ray photoelectron spectroscopy (XPS) and X-ray diffraction (XRD) analysis were used for phase identification. Secondary ion mass spectroscopy (SIMS) and AES were used for depth profile analysis.

Results and Discussion

Oxidation of bare Cu films.—Figure 1 shows the XRD spectra of thermally annealed $Cu/SiO_2/Si$ samples in flowing O_2 ambient. The XRD spectra for the samples annealed at temperatures below 150°C showed no obvious change from that of the as-deposited one. When annealed at temperatures above 175°C, copper oxide phases including Cu_2O and CuO appeared, as illustrated in Fig. 1a; their appearance is entirely consistent with those reported in the literature.[21–23] The increasing signal of Cu_2O phase with increasing annealed time at an annealing temperature of 200°C is illustrated in Fig. 1b. Figure 2 illustrates the percentage change of sheet resistance ($\Delta Rs/Rs$) for the thermally annealed $Cu/SiO_2/Si$ samples. By comparing Fig. 2a with Fig. 1a and by comparing the annealing time dependence of the 200°C annealed sample shown in Fig. 2b with the XRD spectra shown in Fig. 1b, it is found that the increase of sheet resistance corresponded to the appearance of Cu oxide phases in the XRD spectra. At temperatures higher than 200°C, for example 300°C, the oxidation of Cu proceeded quickly, and the sheet resistance rapidly increased (Fig. 2b). When annealed at lower temperatures, for example 100°C, sheet resistance decreased with the increase of annealing time, presumably due to grain growth and sputter damage healing.

Oxidation of Ta-passivated Cu films.—Sample A.—Figures 3 and 4 show the change of sheet resistance and the XRD spectra, respectively, for the thermally annealed Ta-passivated samples of $Ta/Cu/SiO_2/Si$ (sample A). At temperatures up to 400°C, the sheet resistance showed a monotonic decrease, no signal of Cu oxide phase appeared in the XRD spectra. When annealed at 450°C, signals of CuO phase appeared on the XRD spectra and the sheet resistance increased drastically. Figure 5 shows the surface morphology of sample A before and after the thermal annealing. The as-deposited Ta film of 200 Å thickness has a very smooth surface (Fig. 5a) with grain sizes estimated to be in the order of film thickness. No obvious grain growth was observed in the 400°C annealed sample, but a void was found on the surface (Fig. 5b). As the annealing temperature was raised to 450°C, CuO phase appeared and the films became cracked (Fig. 5c) and peeled off from the SiO_2 substrate.

Figure 6 illustrates the XPS surface element survey[39] for the 400°C annealed sample A. By sequential analysis of the surface region before and after Ar ion milling, we observed

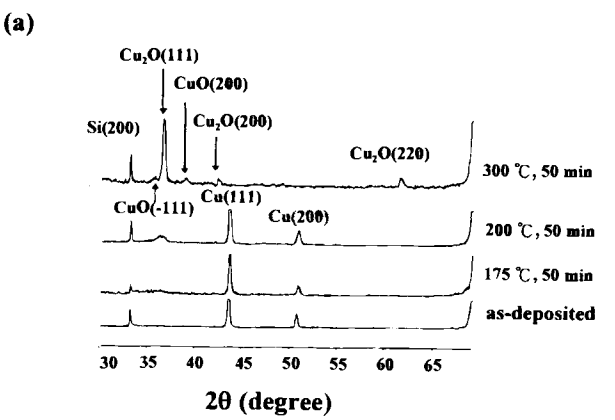

Fig. 1. XRD spectra of bare Cu films thermally annealed in flowing O_2 ambient (a) for 50 min at different temperatures and (b) at 200°C for different periods of time.

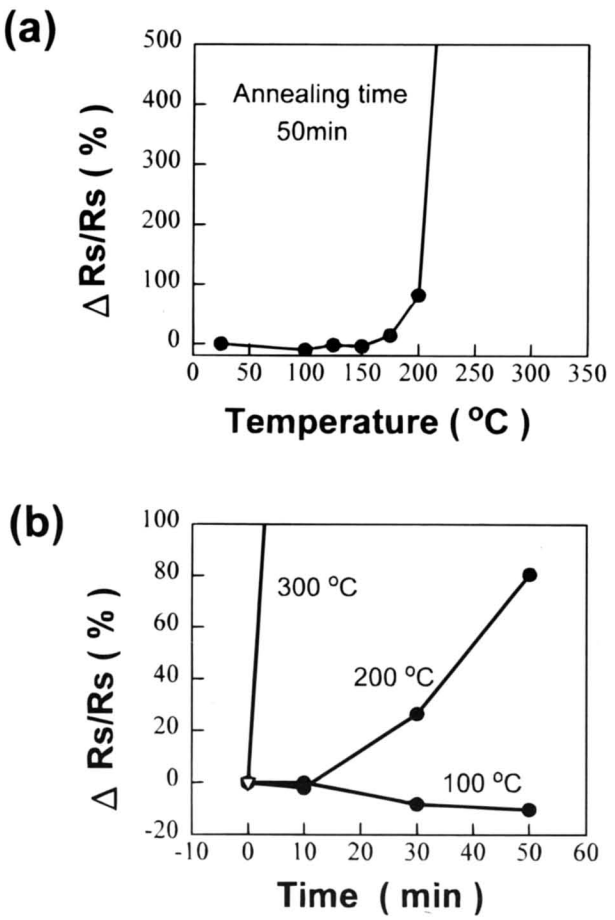

Fig. 2. Sheet resistance change (in percentage) for bare Cu films thermally annealed in flowing O_2 ambient as a function of (a) annealing temperature and (b) annealing time.

similar spectra and found no detectable signal of Cu photoelectron from the outermost surface to the underlying Ta layer. Only photoelectron signals of oxygen and tantalum were found and were determined to be elemental Ta and oxidized Ta (Ta_2O_5) phases. Cu photoelectrons were not detected until the Ta and Ta_2O_5 mixed layer (in short, the Ta–O layer) was ion milled away. These Cu photoelectrons preserved their elemental chemical state, and no oxygen signal was detected in the Cu layer. Figure 7 shows the

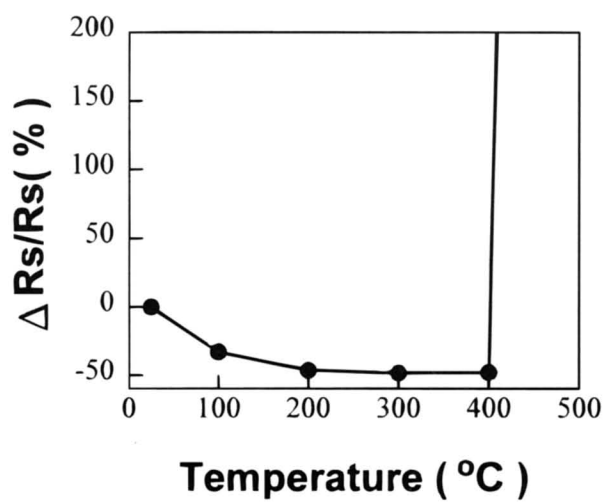

Fig. 3. Sheet resistance change (in percentage) for sample A thermally annealed in flowing O_2 ambient as a function of annealing temperature.

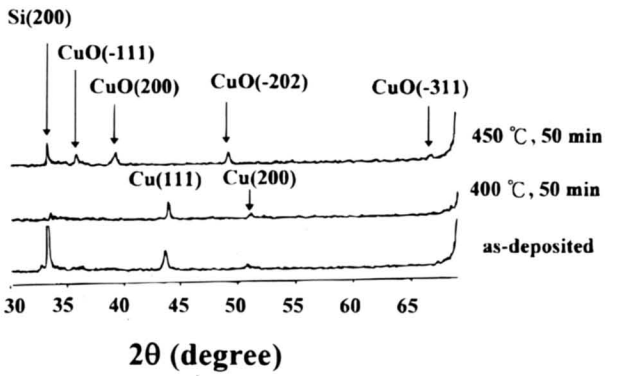

Fig. 4. XRD spectra of sample A before and after thermal anneal in flowing O_2 ambient.

SIMS depth profiles of compositional elements for thermally annealed sample A. The 400°C annealed sample retained the basic passivated structure of Ta–O/Cu/SiO_2

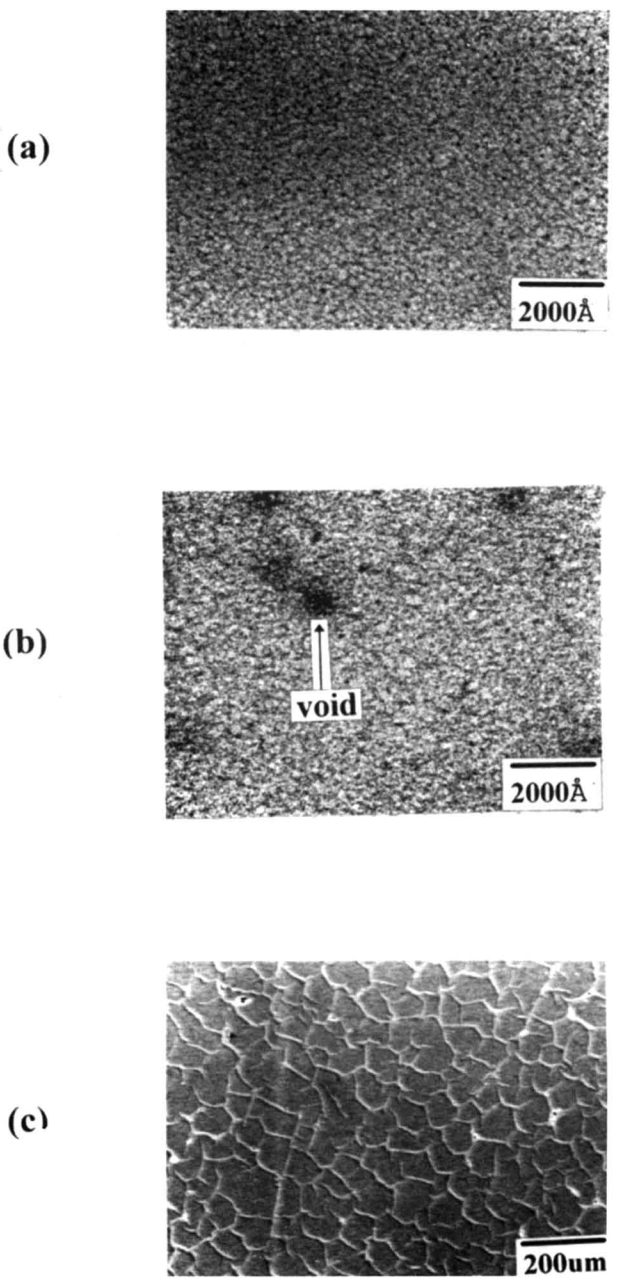

Fig. 5. SEM micrographs showing surface morphology of sample A (a) as-deposited, (b) 400°C annealed, and (c) 450°C annealed.

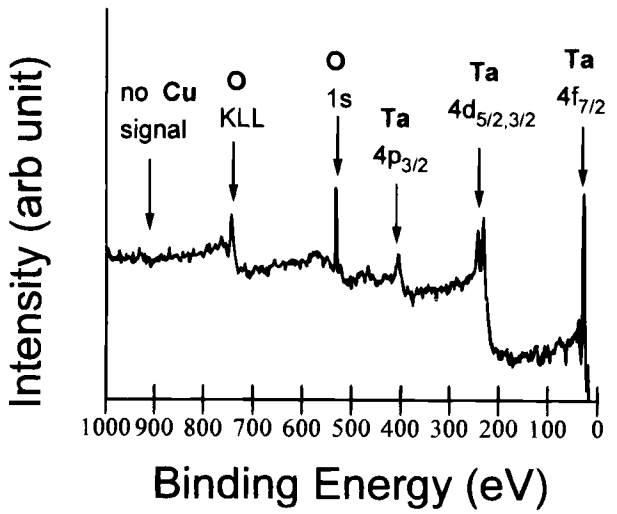

Fig. 6. XPS surface element survey for sample A annealed at 400°C.

(Fig. 7a), instead of pure Ta metal passivated Ta/Cu/SiO_2. After annealing at 450°C, the depth profile showed a layer of CuO (determined by XPS and XRD analysis) in the surface region while Ta was found under the copper oxide layer (Fig. 7b).

The drastic increase of sheet resistance after annealing at temperatures above 400°C is clearly due to the Cu oxidation, while the monotonic decrease of sheet resistance at temperatures below 400°C results from sintering of Cu layer. The voids that appeared on the surface of the 400°C annealed sample (Fig. 5b) were presumably caused by the volume expansion of Ta oxidation.[4,6,7] At temperatures above 400°C, it is presumed that oxidation reaction occurred between oxygen and copper which was thermally out-diffused through the voids and grain boundaries in the Ta and Ta_2O_5 mixed layer. The capability of Ta passivation film against Cu oxidation was found to be higher than 400°C.

Oxidation of Ta–nitride-passivated Cu films.—Sample B.—Figures 8 and 9 show the change of sheet resistance and the XRD spectra, respectively, for the thermally annealed Ta–nitride-passivated sample of Ta-nitride/Cu/SiO_2/Si (sample B). The sheet resistance increased drastically after annealing at 450°C; however, the increase of sheet resistance for sample B is much smaller than that for sample A, and no signal of Cu oxide phase was detected by XRD analysis for the 450°C annealed sample. This suggests that the passivation capability of the nitrogen-doped Ta-nitride film (sample B) is superior to the pure Ta layer (sample A).

Figure 10 shows the AES depth profiles of compositional elements for the 450°C annealed sample B. It can be seen that Cu, O, and Ta all mixed together in the entire measured region. Figure 11 illustrates XPS binding energies of photoelectrons for the surface compositional elements of the 450°C annealed sample B. The Cu $2p_{3/2}$ (Fig. 11a) and O 1s (Fig. 11b) spectra showed that the oxygen photoelectrons were in the Cu_2O state, while the Ta $4f_{7/2}$ (Fig. 11c) and N 1s (Fig. 11d) spectra indicated that the Ta photoelectrons were in the Ta_2N as well as the Ta_2O_5 state.[39–41] This explains the broad spectrum of O 1s photoelectrons (Fig. 11b).[39] The drastic increase of sheet resistance (Fig. 8) was attributed to the mixing of Cu, O, Ta, and N (Fig. 10), presumably the intermixing of Cu_2O, Ta_2O_5, and Ta_2N. The

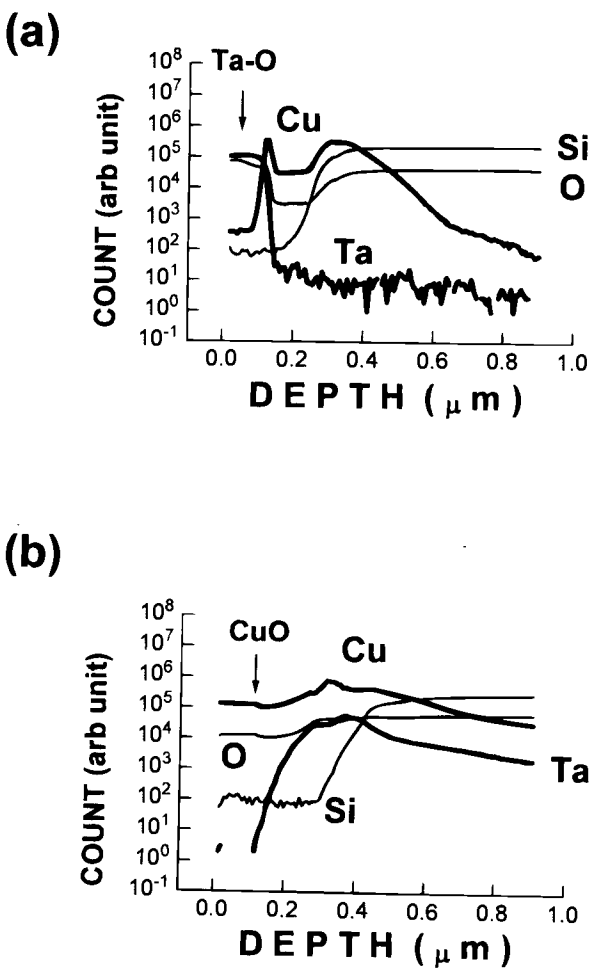

Fig. 7. SIMS depth profiles of compositional elements for sample A annealed at (a) 400 and (b) 450°C.

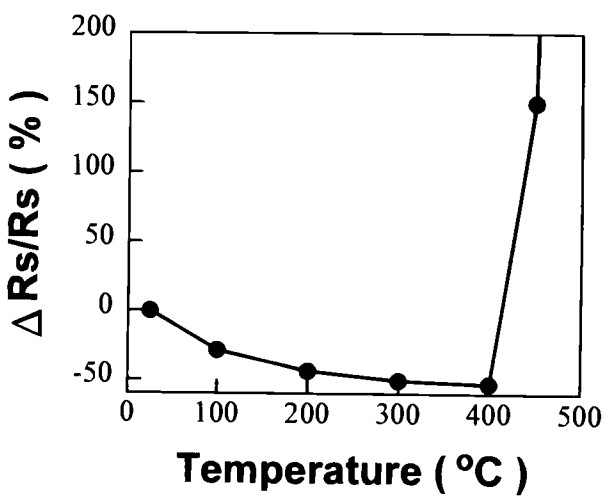

Fig. 8. Sheet resistance change (in percentage) of sample B thermally annealed in flowing O_2 ambient as a function of annealing temperature.

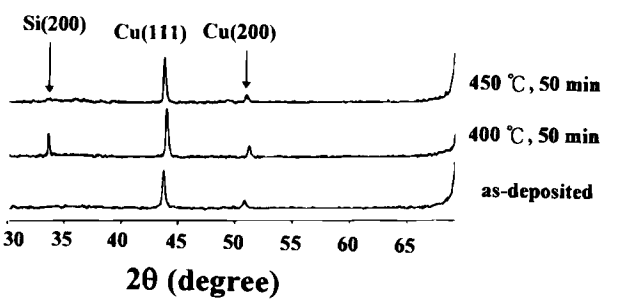

Fig. 9. XRD spectra of sample B before and after thermal anneal in flowing O_2 ambient.

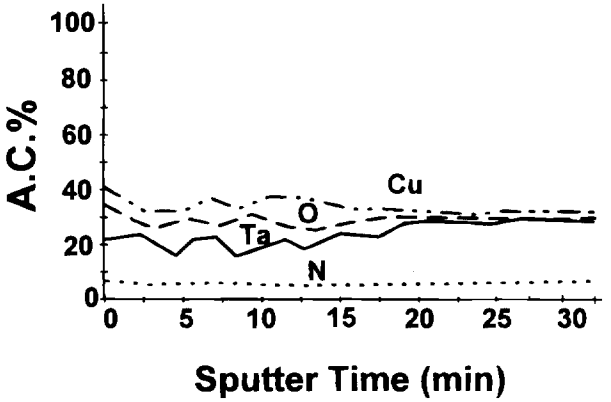

Fig. 10. AES depth profiles of compositional elements for sample B annealed at 450°C.

missing of Cu oxide signal in the XRD spectrum (Fig. 9) suggests that the amount of Cu oxide phase was insignificant except on the surface layer.

Figure 12 shows the surface morphology of the as-deposited sample and the samples annealed at temperatures immediately below as well as above the temperature of drastic sheet resistance change. Voids of various sizes appeared on the surface of 400 and 450°C annealed samples (Fig. 12b and 12c) and presumably arose from the volume difference between Ta-nitrides and Ta oxides.[4,6,7] The Cu_2O cluster[21,22] around the void on the 450°C annealed sample (Fig. 12c) is evidence that Cu is the diffusion species during the oxidation reaction of copper and oxygen.

It was reported that by using the same sputtering condition as employed in this study, the reactively sputtered 500 Å thick Ta–nitride film deposited on Si substrate was nearly amorphous by the XRD analysis, while the sputtered pure Ta film showed distinctly crystallized β-Ta (XRD) peaks.[34] Amorphism was also reported for the Ta_2N layer deposited by reactive rf magnetron sputtering in (Ar + N_2) gas mixture.[37] Nitrogen atoms stuffed[14] in the Ta–nitride grain boundaries might also contribute to the improvement of passivation capability. Nevertheless, we presume that amorphism of the Ta_2N layer was the principal factor of passivation improvement.

Oxidation of Ta-nitride-passivated Cu fims.—Samples C and D.—Figures 13 and 14 show the change of sheet resistance and the XRD spectra, respectively, for the thermally annealed sample C. The monotonic decreasing trend of sheet resistance with annealing temperature stopped at 300°C. After annealing at 400°C, the sheet resistance increased drastically and signals belonging to the CuO phase appeared in the XRD spectrum; moreover, the signal of Cu phase disappeared.

We investigated the 350°C annealed sample in more detail. Figure 15 illustrates the AES depth profiles of compositional elements for sample C annealed at 350°C. It can be seen that the surface of this sample was covered by a layer of mixing elements. This indicates that diffusion of Cu and oxidation of Cu had occurred to some extent, though the XRD spectrum revealed no signal of Cu oxide phase. The XPS analysis showed that the thermally an-

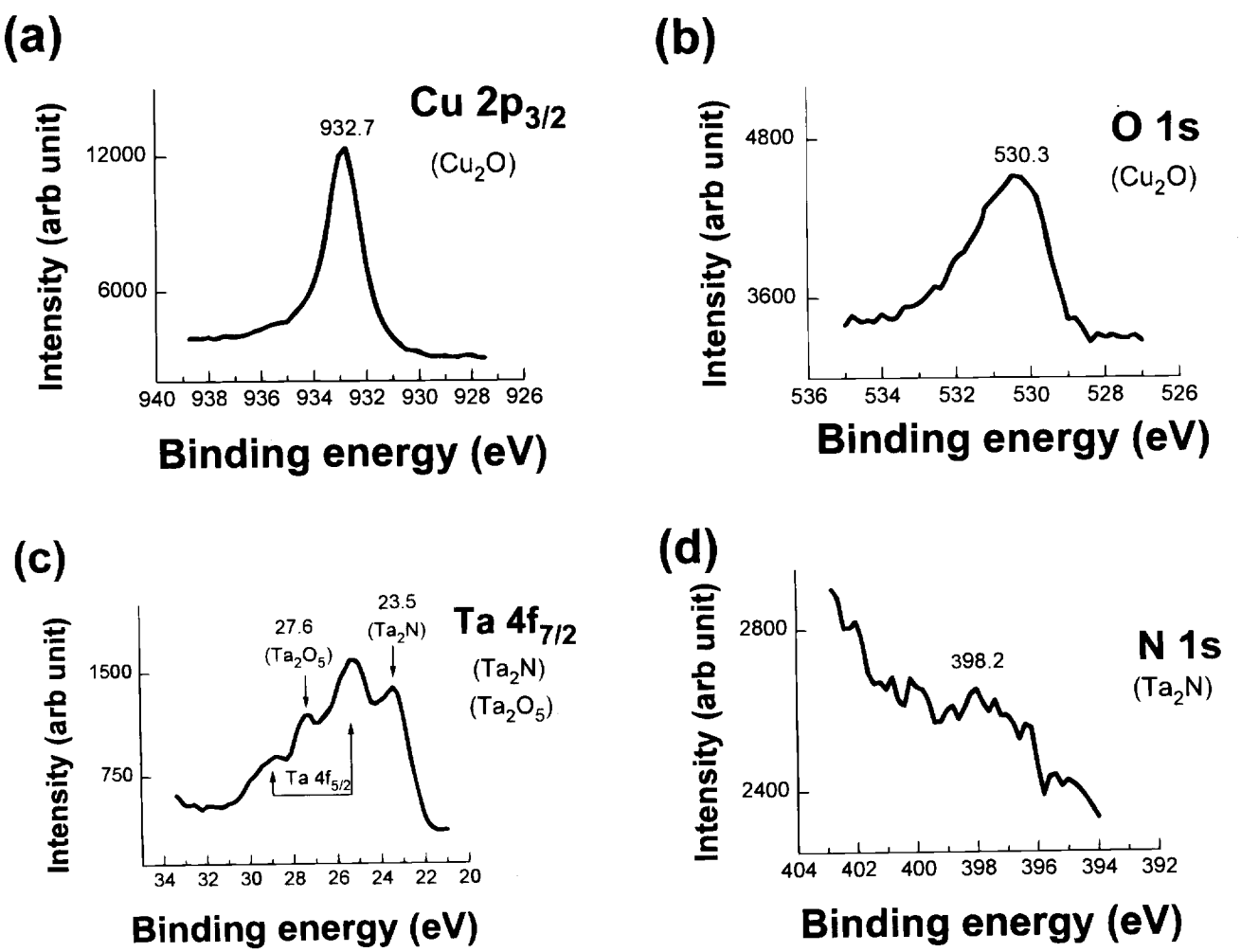

Fig. 11. XPS binding energies of photoelectrons for the surface compositional elements of sample B annealed at 450°C (a) Cu $2p_{3/2}$, (b) O 1s, (c) Ta $4f_{7/2}$, and (d) N 1s.

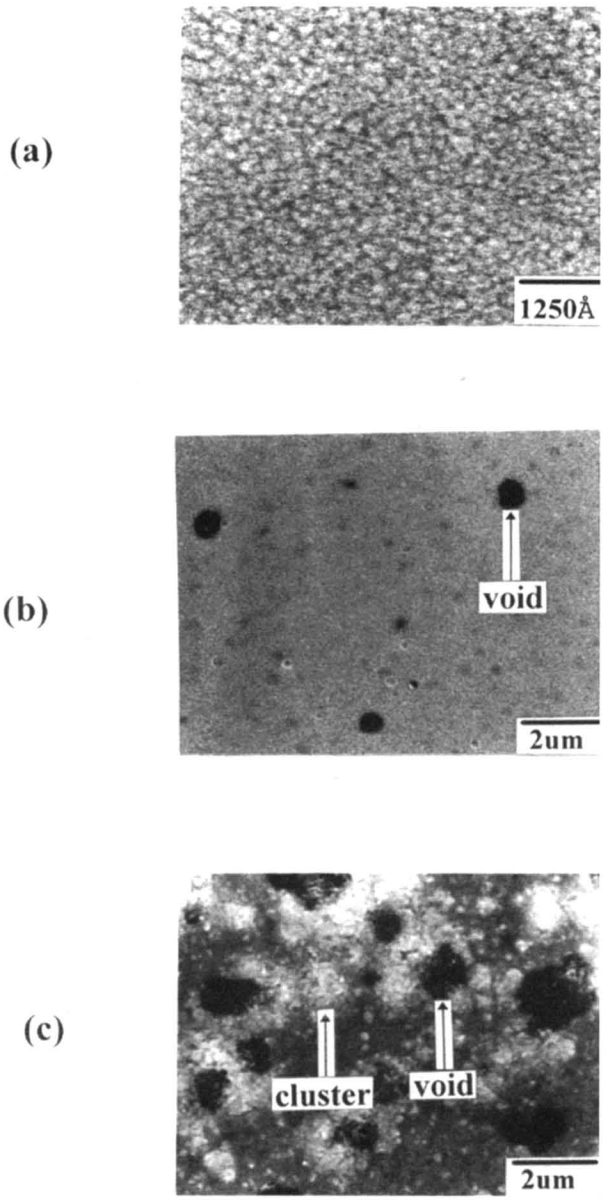

Fig. 12. SEM micrographs showing surface morphology of sample B (a) as-deposited, (b) 400°C annealed, and (c) 450°C annealed.

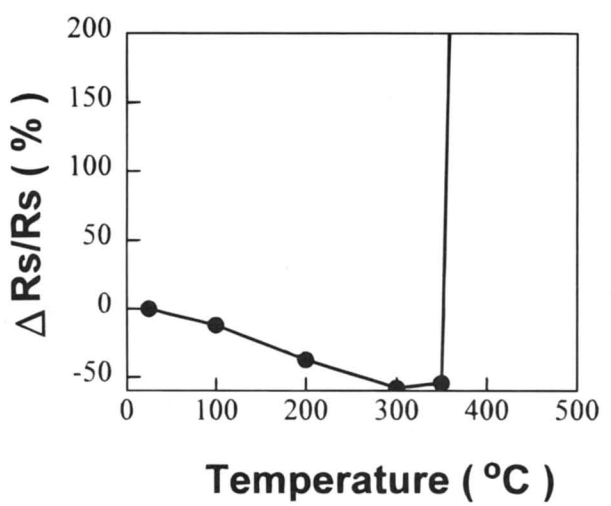

Fig. 13. Sheet resistance change (in percentage) for sample C thermally annealed in flowing O_2 ambient as a function of annealing temperature.

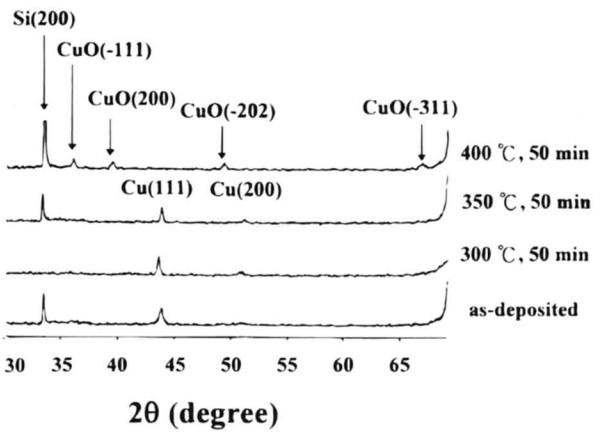

Fig. 14. XRD spectra of sample C before and after thermal anneal in flowing O_2 ambient.

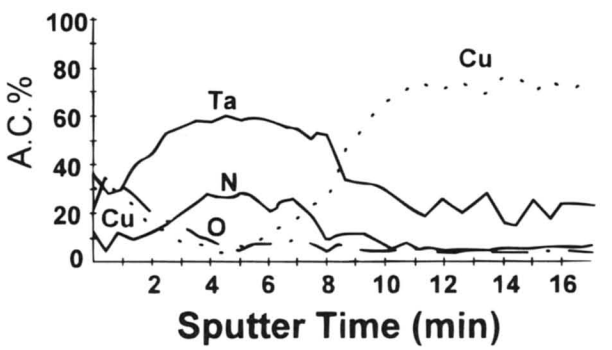

Fig. 15. AES depth profiles of compositional elements for sample C annealed at 350°C.

nealed Ta–nitride remained the same as the as-deposited state of hexagonal TaN.[34,40] Furthermore, oxide phase was detected only on the surface of the passivation layer and was determined to be Cu_2O. It is interesting to observe that the Cu $2p_{3/2}$ photoelectrons underneath the TaN layer remained in the elemental state and that no oxygen signal was detected. This is similar to the thermally annealed sample A in which case once the Ta–nitride-passivated Cu is oxidized, Cu oxides always exist on the outermost surface. This suggests that it is copper, not oxygen, that diffuses through the passivation layer during thermal O_2 annealing of Ta as well at Ta–nitride-passivated Cu films.

From the observations mentioned, it is found that the passivation capability of TaN in sample C was inferior to that of Ta_2N in sample B. Further study on sample D revealed that the passivation capability of Ta–nitride in sample D was even worse than that of TaN in sample C. The poor passivation capability of these highly nitrogen doped Ta–nitride layers was due to film damages, as shown in Fig. 16 for surface morphology of as-deposited samples C and D. These film damages were caused either by excess N_2 plasma in the sputtering process[40] or by tensile stress of the nitrides.[4,7,37] Because of low diffusivity of Cu in Ta and Ta–nitrides at temperatures around 400°C,[4,35] film damages provided the efficient paths for Cu diffusion through the passivation layer. When the sample was thermally annealed the damage healing and the diffusion of Cu through the unhealed defects proceeded simultaneously. For sample C annealed at 350°C, the diffusion of Cu ceased when the defect-related diffusion paths were blocked by the damage healing; thus, Cu_2O was present on the surface and the underlying Cu film retained its integrity (Fig. 15). However, as the annealing temperature was raised to 400°C, CuO formed before the healing of damage (Fig. 14). For sample D, the film damage was so severe (Fig. 16b) that there were a large number of paths for copper and

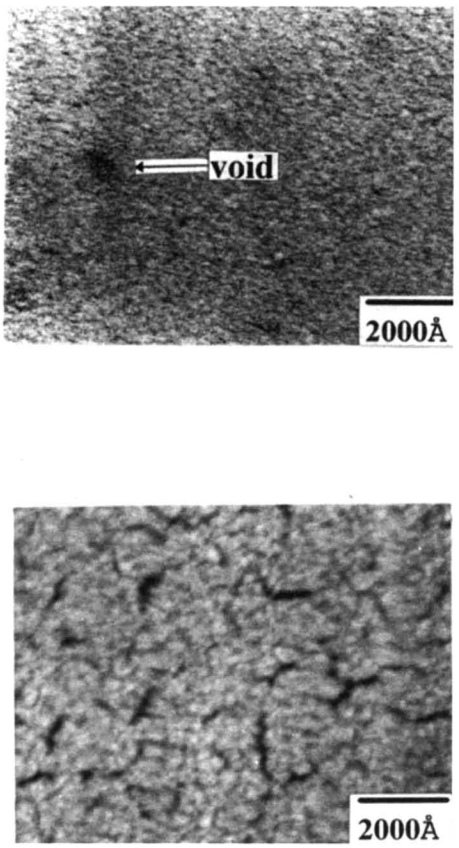

Fig. 16. SEM micrographs showing surface morphology of as-deposited (a) sample C and (b) sample D.

oxygen to diffuse and react with each other; thus, the Ta–nitride layer lost its passivation effect completely.

It has been reported that nitrogen decoration in the grain boundaries of Ta or Ta–nitride film can be beneficial in preventing Cu diffusion.[34–37] In this study, however, amorphous Ta–nitride film of sample B revealed only a modest improvement on the capability of passivation over the Ta film. For samples C and D, whose passivation layers were deposited in Ar/N_2 sputtering gas mixture with higher nitrogen content, the damages or defects containing Ta–nitride films (Fig. 16a for sample C and Fig. 16b for Sample D) degraded the passivation capability. The effect of surface defects caused by excess N_2 plasma in the sputtering gas mixture was further enhanced by the use of very thin (200 Å) films. For practical applications, therefore, there is no benefit from using reactively sputtered Ta–nitride layers. Pure Ta passivation layer can resist oxidizing anneal at 400°C for 50 min without causing oxidation of the underlying copper. However, it is potentially possible to develop a damage healing process to improve the passivation capability of the reactively sputtered Ta–nitride films.

Summary and Conclusion

Sputtered tantalum (Ta) and reactively sputtered Ta–nitride films were studied with respect to the passivation capability against copper (Cu) oxidation in thermal O_2 ambient. A 200 Å Ta or Ta–nitride film was sputter–deposited on a 2000 Å Cu film using a Ta target in an Ar/N_2 gas mixture. The Ta-passivated $Ta/Cu/SiO_2/Si$ structure was able to withstand a thermal annealing in O_2 ambient at 400°C for 50 min without causing Cu oxidation. The use of a Ta–nitride passivation layer sputter–deposited in an appropriate condition further improved the passivation capability. Amorphism of the Ta–nitride film was presumably responsible for this improvement. However, sputter-induced surface damage by excess N_2 in the sputtering gas mixture may degrade the passivation capability of Ta–nitride films, and this effect can be enhanced by the use of very thin films. From the viewpoint of practical applications, therefore, the use of reactively sputtered Ta–nitride film is not necessarily better than that of a pure Ta passivation layer. Whichever we used, once the Ta or Ta–nitride passivated Cu was oxidized, the Cu oxides (CuO or Cu_2O) always existed on the outermost surface. This suggests that it was copper, not oxygen, that diffused through the passivation layer during the thermal O_2 annealing of Ta as well as Ta-nitride passivated Cu films.

Acknowledgments

The authors thank the Semiconductor Research Center of National Chiao-Tung University for providing excellent equipment and processing environment. This study was supported by the National Science Council, ROC, under contact no. NSC-86-2215-E-009-040.

Manuscript submitted October 6, 1997; revised manuscript received May 11, 1998.

National Chiao-Tung University assisted in meeting the publication costs of this article.

REFERENCES

1. See, for example, *MRS Bull.*, **18**(6), (1993) and *MRS Bull.*, **19**(8), (1994), devoted to the topic of *Copper Metallization for Microelectonics*.
2. See, for example, *Thin Solid Films*, **262**, 1995), devoted to a special issue: *Copper-Based Metallization and Interconnects for Ultra-Large-Scale Integration Applications*.
3. K. P. Rodbell, E. G. Colgan, and C-K. Hu, *Mater. Res. Soc. Symp. Proc.*, **337**, 59 (1994).
4. *CRC Handbook of Chemistry and Physics*, 73rd ed., Section 12, D. R. Lide, Editor, CRC Press, Inc., Boca Raton, FL (1992).
5. S. Shingubara, K. Fujiki, A. Sano, H. Sakaue, and Y. Horiike, *Mater. Res. Soc. Symp. Proc.*, **338**, 441 (1994).
6. *Binary Alloy Phase Diagrams*, T. B. Massalski, Editor, 2nd ed., pp. 1446, 1485, 2703, and 2919, ASM International, Metals Park, OH (1990).
7. E. A. Brandes, *Smithells Metals Handbook*, 6th ed., pp. (8-21)-(8-25), Robert Hartnoll, Ltd., Bodmin, Cornwall, England (1983).
8. Y. Igarashi, T. Yamanobe, and T. Ito, *Thin Solid Films*, **262**, 124 (1995).
9. J. D. McBrayer, R. M. Swanson, and T. W. Sigmon, *J. Electrochem. Soc.*, **133**, 1242 (1986).
10. Y. Shacham-Diamand, A. Dedhia, D. Hoffstetter, and W. G. Oldham, *J. Electrochem. Soc.*, **140**, 2427 (1993).
11. D. Gupta, *Mater. Res. Soc. Symp. Proc.*, **337**, 209 (1994).
12. G. Raghavan, C. Chiang, P. B. Anders, S. M. Tzeng, R. Villasol, G. Bai, M. Bohr, and D. B. Fraser, *Thin Solid Films*, **262**, 168 (1995).
13. S. M. Sze, *Physics of Semiconductor Devices*, 2nd ed., Chap. 6–8, John Wiley & Sons, New York (1981).
14. S. Q. Wang, S. Suthar, C. Hoeflich, and B. J. Burrow, *J. Appl. Phys.*, **73**, 2301 (1993).
15. J-C. Chiou, K-C. Juang, and M-C. Chen, *J. Electrochem. Soc.*, **142**, 2326 (1995).
16. J. S. Reid, E. Kolawa, R. P. Ruiz, and M-A. Nicolet, *Thin Solid Films*, **236**, 319 (1993).
17. H. Ono, T. Nakano, and T. Ohta, *Appl. Phys. Lett.*, **64**, 1511 (1994).
18. K-C. Park and K-B. Kim, *J. Electrochem. Soc.*, **142**, 3110 (1995).
19. J. O. Olowolafe, J. Li, J. W. Mayer, and E. G. Colgan, *Appl. Phys. Lett.*, **58**, 469 (1991).
20. A. Noya, M. Takeyama, K. Sasaki, E. Aoyagi, and K. Hiraga, *Jpn. J. Appl. Phys.*, **33**, **Part 1(3A)**, 1528 (1994).
21. J. Li, J. W. Mayer, and E. G. Colgan, *J. Appl. Phys.*, **70**, 2820 (1991).
22. M. O'Reilly, X. Jiang, J. T. Beechinor, S. Lynch, C. Ní Dheasuna, J. C. Patterson, and G. M. Crean, *Appl. Surf. Sci.*, **91**, 152 (1995).
23. H. K. Liou, J. S. Huang, and K. N. Tu, *J. Appl. Phys.*, **77**, 5443 (1995).
24. A. J. Griffin, Jr., S. E. Hernández, and F. K. Brotzen, *J. Electrochem. Soc.*, **141**, 807 (1994).

25. C-K. Hu, B. Luther, F. B. Kaufman, J. Hummel, C. Uzoh, and D. J. Pearson, *Thin Solid Films*, **262**, 84 (1995).
26. W. A. Lanford, P. J. Ding, W. Wang, S. Hymes, and S. P. Murarka, *Thin Solid Films*, **262**, 234 (1995).
27. P. J. Ding, W. Wang, W. A. Lanford, S. Hymes, and S. P. Murarka, *Appl. Phys. Lett.*, **65**, 1778 (1994).
28. J. Li, J. W. Mayer, Y. Schacham-Diamand, and E. G. Colgan, *Appl. Phys. Lett.*, **60**, 2983 (1992).
29. H. Itow, Y. Nakasaki, G. Minamihaba, K. Suguro, and H. Okano, *Appl. Phys. Lett.*, **63**, 934 (1993).
30. D. S. Gardner, J. Onuki, K. Kudoo, Y. Misawa, and Q. T. Vu, *Thin Solid Films*, **262**, 104 (1995).
31. Y. Igarashi, T. Yamanobe, T. Yamaji, S. Nishikawa, and T. Ito, *Jpn. J. Appl. Phys.*, **33**, **Part 1 (1B)**, 462 (1994).
32. S. Hymes, S. P. Murarka, C. Shepard, and W. A. Lanford, *J. Appl. Phys.*, **71**, 4623 (1992).
33. P. J. Ding, W. A. Lanford, S. Hymes, and S. P. Murarka, *J. Appl. Phys.*, **74**, 1331 (1993).
34. D. D. Wu, M.S. Thesis, National Chiao-Tung University, Hsinchu, Taiwan (1996).
35. K. Holloway, P. M. Fryer, C. Cabral, Jr., J. M. E. Harper, P. J. Bailey, and K. H. Kelleher. *J. Appl. Phys.*, **71**, 5433 (1992).
36. T. Nakano, H. Ono, T. Ohta, T. Oku, and M. Murakami, *1994 VMIC Conference Proceeding*, 407 (1994).
37. X. Sun, E. Kolawa, J-S. Chen, J. S. Reid, and M-A. Nicolet, *Thin Solid Films*, **236**, 347 (1993).
38. W. Kern and D. A. Puotinen, *RCA Rev.*, **31**, 187 (1970).
39. *Handbook of X-Ray Photoelectron Spectroscopy*, G. E. Muilenberg, Editor, Perkin-Elmer Corporation, Physical Electronics Division, Eden Prairie, MN (1978).
40. J-C. Chuang and M-C. Chen, *Thin Solid Films*, To be published (1998).
41. K. Baba and R. Hatada, *Surf. Coat. Technol.*, **84**, 429 (1996).

Intermediate Temperature Solid Oxide Fuel Cells Using a New $LaGaO_3$ Based Oxide Ion Conductor

I. Doped $SmCoO_3$ as a New Cathode Material

Tatsumi Ishihara,* Miho Honda, Takaaki Shibayama, Hiroaki Minami, Hiroyasu Nishiguchi, and Yusaku Takita

Department of Applied Chemistry, Faculty of Engineering, Oita University, Oita 870-1121, Japan

ABSTRACT

$LaGaO_3$-based perovskite oxides doped with Sr and Mg exhibit high ionic conductivity over a wide range of oxygen partial pressure. In this study, the stability of $LaGaO_3$-based oxide was investigated. The $LaGaO_3$-based oxide was found to be very stable in reducing, oxidizing, and CO_2 atmospheres. Solid oxide fuel cells (SOFCs) using $LaGaO_3$-based perovskite-type oxide as the electrolyte were studied for use in intermediate-temperature SOFCs. The power-generation characteristics of cells were strongly affected by the electrodes. Both Ni and $LnCoO_3$ (Ln:rare earth) were suitable for use as anode and cathode, respectively. Rare-earth cations in the Ln site of the Co-based perovskite cathode also had a significant effect on the power-generation characteristics. In particular, a high power density could be attained in the temperature range 973–1273 K by using a doped $SmCoO_3$ for the cathode. Among the examined alkaline earth cations, Sr-doped $SmCoO_3$ exhibits the smallest cathodic overpotential resulting in the highest power density. The electrical conductivity of $SmCoO_3$ increased with increasing Sr doped into the Sm site and attained a maximum at $Sm_{0.5}Sr_{0.5}CoO_3$. The cathodic overpotential and internal resistance of the cell exhibited almost the opposite dependence on the amount of doped Sr. Consequently, the power density of the cell was a maximum when $Sm_{0.5}Sr_{0.5}CoO_3$ was used as the cathode. For this cell, the maximum power density was as high as 0.58 W/cm^2 at 1073 K, even though a 0.5 mm thick electrolyte was used. This study revealed that a $LaGaO_3$-based oxide for electrolyte and a $SmCoO_3$-based oxide for the cathode are promising components for SOFCs operating at intermediate temperature.

Introduction

SOFCs provide a new and clean electric power generation system. At present, Y_2O_3-stabilized ZrO_2 (YSZ) is commonly used as the electrolyte of the SOFC. Because the oxide-ion conductivity of YSZ is insufficient for the electrolyte of fuel cells, a thin electrolyte film without gas leakage, and an excessively high operating temperature such as 1273 K are essential for achieving the high power density of SOFCs when YSZ is used as electrolyte. All advantages of SOFC, such as high efficiency and a variety of usable fuel, can be obtained at decreased temperatures such as 1073 K. Furthermore, the choice of the materials for cell stacking becomes wider; in particular, inexpensive refractory metals such as a stainless steel become usable by decreasing the operating temperature to 1100 K. Consequently, a decrease in operating temperature is of great importance for the development of inexpensive but reliable cells.[1] Decreasing the operating temperature requires an active electrode, i.e., a cathode catalyst, and an electrolyte with low resistance. Ceria doped with Gd or Sm is under investigation for the electrolyte of SOFCs operable in a decreased temperature range.[1] However, ceria-based oxides exhibit n-type semiconduction in a reducing atmosphere,[2] which significantly decreases the open-circuit potential from the theoretical value.[3] In addition, some fuel is consumed by leaking oxygen due to an internal short-circuited state of electrolytes due to the presence of free electrons. It is also reported that expansion due to reduction causes severe stress on electrolytes, which sometimes becomes higher than the intrinsic mechanical strength of CeO_2 electrolyte.[4,5] Therefore, there are some problems which should be solved for a CeO_2-based oxide cell. The preparation of very thin YSZ films is also being investigated for intermediate-temperature SOFCs;[6] however, reliability becomes low when the thickness of electrolytes becomes extremely thin and it is furthermore anticipated that power density may become unstable by using a very thin YSZ film for the electrolyte. In the case of YSZ, it is reported that the oxide-ion conductivity decreases gradually with time.[7] This phenomenon is called an annealing effect and seems to be caused by a phase transition from a stabilized cubic phase to a tetragonal phase or changes in grain-boundary properties.[7] The phase transition is a diffusion-controlled process, and hence, the degradation of the ionic conductivity could be pronounced in the case of an excessively thin film.

It is therefore of great importance to develop new electrolyte materials which exhibit high oxide ion conduction over a wide oxygen partial pressure range. Reports on ox-

* Electrochemical Society Active Member.